

See discussions, stats, and author profiles for this publication at: <https://www.researchgate.net/publication/24264606>

High-Performance Air-Stable n-Channel Organic Thin Film Transistors Based on Halogenated Perylene Bisimide Semiconductors

ARTICLE *in* JOURNAL OF THE AMERICAN CHEMICAL SOCIETY · MAY 2009

Impact Factor: 12.11 · DOI: 10.1021/ja901077a · Source: PubMed

CITATIONS

301

READS

46

11 AUTHORS, INCLUDING:



[Wen-Ya Lee](#)

National Taipei University of Technology

60 PUBLICATIONS 1,442 CITATIONS

[SEE PROFILE](#)



[Krzysztof Radacki](#)

University of Wuerzburg

271 PUBLICATIONS 5,502 CITATIONS

[SEE PROFILE](#)



[Holger Braunschweig](#)

University of Wuerzburg

534 PUBLICATIONS 10,455 CITATIONS

[SEE PROFILE](#)

High-Performance Air-Stable n-Channel Organic Thin Film Transistors Based on Halogenated Perylene Bisimide Semiconductors

Rüdiger Schmidt,[†] Joon Hak Oh,[‡] Ya-Sen Sun,[‡] Manuela Deppisch,[†] Ana-Maria Krause,[†] Krzysztof Radacki,[†] Holger Braunschweig,[†] Martin Könemann,[#] Peter Erk,[#] Zhenan Bao,^{*,‡} and Frank Würthner^{*,†}

Universität Würzburg, Institut für Organische Chemie and Institut für Anorganische Chemie und Röntgen Research Center for Complex Material Systems, Am Hubland, D-97074 Würzburg, Germany, Department of Chemical Engineering, 381 North South Mall, Stanford University, Stanford, California 95305, and BASF SE, 67056 Ludwigshafen, Germany

Received February 11, 2009; E-mail: wuerthner@chemie.uni-wuerzburg.de; zbao@stanford.edu

Abstract: The syntheses and comprehensive characterization of 14 organic semiconductors based on perylene bisimide (PBI) dyes that are equipped with up to four halogen substituents in the bay area of the perylene core and five different highly fluorinated imide substituents are described. The influence of the substituents on the LUMO level and the solid state packing of PBIs was examined by cyclic voltammetry and single crystal structure analyses of seven PBI derivatives, respectively. Top-contact/bottom-gate organic thin film transistor (OTFT) devices were constructed by vacuum deposition of these PBIs on SiO₂ gate dielectrics that had been pretreated with *n*-octadecyl triethoxysilane in vapor phase (OTS-V) or solution phase (OTS-S). The electrical characterization of all devices was accomplished in a nitrogen atmosphere as well as in air, and the structural features of thin films were explored by grazing incidence X-ray diffraction (GIXD) and atomic force microscopy (AFM). Several of those PBIs that bear only hydrogen or up to two fluorine substituents at the concomitantly flat PBI core afforded excellent n-channel transistors, in particular, on OTS-S substrate and even in air ($\mu > 0.5 \text{ cm}^2 \text{ V}^{-1} \text{ s}^{-1}$; $I_{on}/I_{off} > 10^6$). The best OTFTs were obtained for 2,2,3,3,4,4,4-heptafluorobutyl-substituted PBI **1a** (“PTCDI-C4F7”) on OTS-S with n-channel field effect mobilities consistently $> 1 \text{ cm}^2 \text{ V}^{-1} \text{ s}^{-1}$ and on-to-off current ratios of 10^6 in a nitrogen atmosphere and in air. For distorted core-tetrahalogenated (fluorine, chlorine, or bromine) PBIs, less advantageous solid state packing properties were found and high performance OTFTs were obtained from only one tetrachlorinated derivative (**2d** on OTS-S). The excellent on-to-off current modulation combined with high mobility in air makes these PBIs suitable for a wide range of practical applications.

Introduction

Organic semiconductors are key components of numerous electronic and optoelectronic devices with various applications, including photovoltaic cells, light-emitting diodes, and organic thin-film transistors (OTFTs).¹ Historically, the performance of n-type organic semiconductors was outmatched by that of the more intensively investigated p-type materials. Nevertheless, both kinds of semiconductors are required for the fabrication of complementary integrated circuits, bipolar transistors, or organic p/n junctions. During the past few years a larger number of organic materials have been reported that surpass the electron mobilities of amorphous silicon. In most cases, these electron deficient semiconductors have been designed by introducing electron withdrawing groups to extended aromatic π -systems with good p-channel activity. Appreciably high electron mobilities have been reported for oligothiophenes² ($0.60 \text{ cm}^2 \text{ V}^{-1} \text{ s}^{-1}$)

and thiazole³ ($1.83 \text{ cm}^2 \text{ V}^{-1} \text{ s}^{-1}$) derivatives containing perfluorinated substituents.⁴ Core fluorination of copper phthalocyanines⁵ has provided n-type materials, which display mobilities

- (1) For representative reviews on organic transistors, see: (a) Katz, H. E.; Bao, Z.; Gilat, S. L. *Acc. Chem. Res.* **2001**, *34*, 359–369. (b) Dimitrakopoulos, C. D.; Malenfant, P. R. L. *Adv. Mater.* **2002**, *14*, 99–117. (c) Bendikov, M.; Wudl, F.; Perepichka, D. F. *Chem. Rev.* **2004**, *104*, 4891. (d) Newman, C. R.; Frisbie, C. D.; da Silva Filho, D. A.; Bredas, J.-L.; Ewbank, P. C.; Mann, K. R. *Chem. Mater.* **2004**, *16*, 4436–4451. (e) Bredas, J.-L.; Beljonne, D.; Coropceanu, V.; Cornil, J. *Chem. Rev.* **2004**, *104*, 4971–5004. (f) Würthner, F.; Schmidt, R. *ChemPhysChem.* **2006**, *7*, 793–797. (g) Anthony, J. E. *Chem. Rev.* **2006**, *106*, 5028–5048. (h) Klauk, H., Ed. *Organic Electronics*; Wiley-VCH: Weinheim, Germany, 2006. (i) Bao, Z.; Locklin, J., Eds. *Organic Field-Effect Transistors*; Taylor and Francis: Boca Raton, FL, 2007. (j) Facchetti, A. *Mater. Today* **2007**, *10*, 28–37. (k) Mori, T. *J. Phys.: Condens. Matter* **2008**, *20*, 184010. (l) Mas-Torrent, M.; Rovira, C. *Chem. Soc. Rev.* **2008**, *37*, 827–838. (m) Braga, D.; Horowitz, G. *Adv. Mater.* **2009**, *21*, 1–14. For reviews on organic solar cells, see: (n) special issue of *Materials Today* **2007**, (November) *10*. For reviews on organic light-emitting diodes, see: (o) Müllen, K.; Scherf, U., Eds. *Organic Light Emitting Devices, Synthesis, Properties and Applications*; Wiley-VCH: Weinheim, Germany, 2005.
- (2) (a) Yoon, M.; DiBenedetto, S. A.; Facchetti, A.; Marks, T. J. *J. Am. Chem. Soc.* **2005**, *127*, 1348–1349. (b) Yoon, M.; Facchetti, A.; Stern, C. E.; Marks, T. J. *J. Am. Chem. Soc.* **2006**, *128*, 5792–5801.

[†] Universität Würzburg.

[‡] Stanford University.

[#] BASF SE.

of up to $0.03 \text{ cm}^2 \text{ V}^{-1} \text{ s}^{-1}$. Perfluorinated pentacene shows electron mobilities of up to $0.11 \text{ cm}^2 \text{ V}^{-1} \text{ s}^{-1}$.⁶ With cyano-substituted terthienoquinoid derivatives,⁶ field effect mobilities of up to $0.16 \text{ cm}^2 \text{ V}^{-1} \text{ s}^{-1}$ have been obtained, even in spin-coated devices. Fullerene⁷ (C_{60}) represents one of the few examples of known n-type organic semiconductors without additional electron-withdrawing groups, and it exhibits electron mobilities greater than $0.1 \text{ cm}^2 \text{ V}^{-1} \text{ s}^{-1}$. Remarkable electron mobilities (up to $2.10 \text{ cm}^2 \text{ V}^{-1} \text{ s}^{-1}$)⁸ were also measured for various perylene bisimide (PBI) dyes. As PBIs can be readily synthesized, these semiconductors are among the most promising candidates for molecular design to approach the high-performance requirements.

One grave drawback of most n-channel semiconductors described in the literature so far is the lack of stability of devices operated under ambient conditions in air. Various factors influencing the stability of OTFT devices are still a subject of intense research.^{9,10} In a recent study on cyano PBIs, Jones et al. have demonstrated that the thermodynamic stability of the generated charge carriers alone can hardly explain the observed stability of devices prepared from these materials, because a reduction potential greater than $+0.57 \text{ V}$ vs SCE ($+0.10 \text{ V}$ vs ferrocene) would be required to avoid oxidation of the negative charge carriers by oxygen.⁹ Such high reduction potentials have not been realized with any PBI derivative yet. However, an overpotential, postulated previously by deLeeuw et al. for doped polymers,¹¹ seems to hinder the oxidation of dye radical anions leading to air-stable OTFT operation for PBIs with $E^{\text{red}} > -0.1 \text{ V}$ vs SCE ($> -0.6 \text{ V}$ vs ferrocene) according to Jones et al.⁹

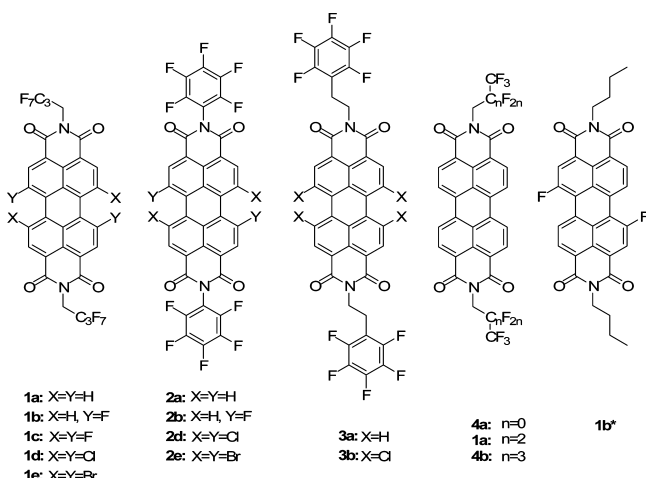
A kinetic approach toward air-stable n-channel semiconductors is the design of compounds in which segregated side chains prevent the intrusion of oxygen and moisture into the active layer. This concept had been intensively studied for rylene bisimide dyes containing perfluorinated substituents in the imide

positions.^{12–14} Exposure to humidity and oxygen did not decrease the performance of such field-effect transistors significantly. The air stability of these compounds was attributed to the dense self-segregation of the fluoro alkyl chains that hinders the diffusion of oxygen into the channel region. Based on the measured X-ray structures of various PBI derivatives, it has been demonstrated that this segregation is less compact in halogen-free systems containing the corresponding alkyl chains in the imide positions. Because the LUMO energy of most materials bearing fluorinated alkyl or phenyl groups is far too high ($E^{\text{red}} < -0.1 \text{ V}$ vs SCE) to prevent the oxidation of corresponding anions, the air stability of such materials cannot be explained only by electronic grounds. However, Klauk and co-workers¹⁰ have recently shown that the above-mentioned kinetic model cannot adequately explain the stability or instability of this class of materials, and a subtle interplay between electronic and kinetic factors seems to determine the ambient stability of PBI semiconductors. To-date, the best mobilities and stabilities have been obtained with PBI derivatives by combining both concepts. Thus, a core-cyanated perylene dye with perfluorobutyl groups in the imide positions showed air-stable mobilities of $0.64 \text{ cm}^2 \text{ V}^{-1} \text{ s}^{-1}$.¹⁴ Unfortunately, the very low reduction potential of this substance allows the existence of radical anions in the thin layers already without applying any gate voltage, and hence leading to “always on” transistors.

Nevertheless, perylene bisimide dyes belong to the most auspicious candidates for electronic applications. The solid state packing and the functional properties of PBIs can be further tailored either by introduction of appropriate substituents in the imide position or by core substitution in the bay region,^{15–22} and merely a fraction of potential PBI derivatives has been investigated so far in regard to their electronic applications. To gain a deeper understanding of the relationship between molecular structure, electronic properties, solid-state packing, and OTFT characteristics, including the ambient stability of devices, we have synthesized a broad spectrum of core-halogenated PBIs with varying fluorinated imide substituents (Chart 1).

Here we present our detailed studies with these PBIs aimed at a better comprehension of the influence of bay and imide substituents of perylene dyes on the crystal packing and their use as n-type organic semiconductors in electronic devices. Single crystal structural data of seven compounds could be obtained, and the electronic properties of all soluble PBI derivatives were investigated by cyclic voltammetry and UV-vis spectroscopy. The morphologies of thin films of these PBIs were examined with grazing incidence X-ray diffraction (GIXD) and atomic force microscopy (AFM) measurements, and charge carrier mobilities were evaluated in the corresponding OTFT devices. The mobilities of compounds **1a**, **1b**, and **1c** were previously reported.^{18–20} However, the performance of the OTFTs has been further improved by dielectric surface engi-

- (3) Ando, S.; Muratami, R.; Nishida, J.; Tada, H.; Inoue, Y.; Tokito, S.; Yamashita, Y. *J. Am. Chem. Soc.* **2005**, *127*, 14996–14997.
- (4) Kono, T.; Kumaki, D.; Nishida, J.-I.; Sakanoue, T.; Kakita, M.; Tada, H.; Tokito, S.; Yamashita, Y. *Chem. Mater.* **2007**, *19*, 1218–1220.
- (5) Bao, Z.; Lovinger, A.; Brown, J. *J. Am. Chem. Soc.* **1998**, *120*, 207–208.
- (6) Handa, S.; Miyazaki, E.; Takimiya, K.; Kunugi, Y. *J. Am. Chem. Soc.* **2007**, *129*, 11684–11685.
- (7) (a) Lee, T. W.; Byun, Y.; Koo, B. W.; Kang, I. N.; Lyu, Y. Y.; Lee, C. H.; Lee, S. Y. *Adv. Mater.* **2005**, *17*, 2180–2184. (b) Meijer, E. J.; de Leeuw, D. M.; Setayesh, S.; Veenendaal, E.; Huisman, B. H.; Blom, P. W. M.; Hummelen, J. C.; Scherf, U.; Klapwijk, T. M. *Nat. Mater.* **2003**, *2*, 678–682. (c) Kobayashi, S.; Takenobu, T.; Mori, S.; Fujiwara, A.; Iwasa, Y. *Appl. Phys. Lett.* **2003**, *82*, 4581–4583. (d) Itaka, K.; Yamashiro, M.; Yamaguchi, J.; Haemori, M.; Yaginuma, S.; Matsumoto, Y.; Kondo, M.; Koinuma, H. *Adv. Mater.* **2006**, *18*, 1713–1716. (e) Anthopoulos, T. D.; Singh, B.; Marjanovic, N.; Sariciftci, N. S.; Ramil, A. M.; Sitter, H.; Cölle, M.; de Leeuw, D. M. *Appl. Phys. Lett.* **2006**, *89*, 213504.
- (8) (a) Tatemichi, S.; Ichikawa, M.; Koyama, T.; Taniguchi, Y. *Appl. Phys. Lett.* **2006**, *89*, 112108. (b) Chesterfield, R. J.; McKeen, J. C.; Newman, C. R.; Ewbank, P. C.; da Silva Filho, D. A.; Bredas, J.-L.; Miller, L. L.; Mann, K. R.; Frisbie, C. D. *J. Phys. Chem. B* **2004**, *108*, 19281–19292. (c) Malenfant, P. R. L.; Dimitrakopoulos, C. D.; Gelorme, J. D.; Kosbar, L. L.; Graham, T. O.; Curioni, A.; Andreoni, W. *Appl. Phys. Lett.* **2002**, *80*, 2517–2519.
- (9) (a) Jones, B. A.; Facchetti, A.; Wasielewski, M. R.; Marks, T. J. *J. Am. Chem. Soc.* **2007**, *129*, 15259–15278. (b) Jones, B. A.; Facchetti, A.; Wasielewski, M. R.; Marks, T. J. *Adv. Funct. Mater.* **2008**, *18*, 1329–1339.
- (10) Weitz, R. T.; Amsharov, K.; Zschieschang, U.; Villas, E. B.; Goswami, D. K.; Burghard, M.; Dosch, H.; Jansen, M.; Kern, K.; Klauk, H. *J. Am. Chem. Soc.* **2008**, *130*, 4637–4645.
- (11) deLeeuw, D. M.; Simenon, M. M. J.; Brown, A. R.; Einerhand, R. E. F. *Synth. Met.* **1997**, *87*, 53–59.
- (12) (a) Katz, H. E.; Lovinger, A. J.; Johnson, J.; Kloc, C.; Slegrist, T.; Li, W.; Lin, Y.-Y.; Dodabalapur, A. *Nature (London)* **2000**, *404*, 478–481. (b) Würthner, F. *Angew. Chem., Int. Ed.* **2001**, *40*, 1037–1039.
- (13) Chen, H. Z.; Ling, M. M.; Mo, X.; Shi, M. M.; Wang, M.; Bao, Z. *Chem. Mater.* **2007**, *19*, 816–824.
- (14) Jones, A. J.; Ahrens, M. J.; Yoon, M.-H.; Facchetti, A.; Marks, T. J.; Wasielewski, M. R. *Angew. Chem., Int. Ed.* **2004**, *43*, 6363–6366.
- (15) Osswald, P.; Würthner, F. *J. Am. Chem. Soc.* **2007**, *129*, 14319–14326.
- (16) Würthner, F. *Chem. Commun.* **2004**, 1564–1579.
- (17) Qiu, W.; Chen, S.; Sun, X.; Liu, Y.; Zhu, D. *Org. Lett.* **2006**, *8*, 867–870.
- (18) Schmidt, R.; Ling, M.-M.; Oh, J. H.; Winkler, M.; Könemann, M.; Bao, Z.; Würthner, F. *Adv. Mater.* **2007**, *19*, 3692–3695.

Chart 1. Structures of Perylene Bisimides Investigated Here

neering. The dyes of series **1** and **2** are decorated with fluorinated alkyl and phenyl imide substituents,^{13,14,21} while in each of these series the core substituents (fluorine, chlorine, and bromine) are varied as the bay substitution has a large impact on the packing features of PBI dyes in the solid state. Furthermore, strong electron withdrawing-groups change the redox potentials (and LUMO energies) of these dyes significantly, which influence not only the semiconducting properties but also electron injection barriers into these materials. The unsubstituted dyes **1a** and **2a** are included for comparison; the latter derivative has been reported before, and it shows air-stable mobilities of $0.06 \text{ cm}^2 \text{ V}^{-1} \text{ s}^{-1}$.¹³ Derivative **1b*** has the same PBI core as **1b** but lacks fluorine substituents in the imide side chains. Perfluorinated alkyl amines of different lengths (series **4**) were chosen to elucidate the influence of chain length on packing and device performance, while the compounds **3** are modifications of the BASF “black pigment” which also proved to be an air-stable high performance n-channel semiconductor.²²

Results and Discussion

Synthesis of PBIs 1–4. The PBI derivatives investigated in this work were synthesized according to Scheme 1. Starting materials **5a** and **5b** were provided by the BASF SE, and the bisanhydrides **5c**²³ and **5d** (isolated in isomerically pure form)²⁴ were synthesized according to literature procedures. For the synthesis of PBIs **1a**, **1d**–**1f**, **3b**, **4a**, and **4b**, a previously reported imidization procedure was chosen, employing *N*-methyl-2-pyrrolidone (NMP) together with catalytic amounts of acetic acid as solvent.¹⁴ Due to the very low nucleophilicity of pentafluoroaniline, a large excess of the amine with catalytic amounts of acetic acid in NMP had to be used for the synthesis of **2d**–**f**. Because of the low reactivity of fluorinated amines and poor solubility of monoimidized intermediate products,

imidization afforded in some cases low yield (e.g., for **4b** 13%). Core-fluorinated PBIs **1b** and **1c** were obtained by Halex reaction²⁵ of the corresponding dibrominated PBI **1f** and tetrachlorinated PBI **1d** with potassium chloride in sulfolane as solvent and in the presence of 18-crown-6 (for **1b**) or *N,N'*-dimethylimidazolidino-tetramethylguanidinium chloride (CNC⁺) (for **1c**) as catalyst in 32% and 8.6% isolated yield, respectively. The relatively low yield of **1c** is due to the formation of large amounts of only partially fluorinated intermediary products, which could be isolated and reused. PBI **2a** was synthesized as described in the literature.¹³ PBI **3a** was synthesized by imidization in quinoline using zinc acetate as catalyst. The detailed synthetic procedures and characterization data of the PBI derivatives are given in the Supporting Information.

Electrochemical Properties of 1–4. The soluble PBI derivatives were characterized by cyclic voltammetry, and the results are summarized in Table 1. These dyes exhibit two reversible reduction waves, while no oxidation wave could be observed due to the limited available potential range in the given solvent. Exemplary cyclic voltammograms of the unsubstituted PBI **1a** and the most electron-deficient PBI **2e** are shown in the Supporting Information (Figure S1). The first reduction potentials of compounds **1** range from -0.95 eV (**1a**) to -0.70 eV (**1e**) (Table 1). Compared with other halogen-free alkyl-substituted PBIs (e.g., cyclohexyl) that lack core substituents ($E(\text{PBI}/\text{PBI}^-) \approx -1.10 \text{ eV}$),¹⁶ dye **1a** can be reduced more easily by $\sim 150 \text{ mV}$ due to the electron-withdrawing effect of the perfluorinated butyl substituent. Bromine substitution of the core (**1e**) has an even stronger effect on the reduction potential, which is increased by 400 mV in comparison to that of the halogen-free derivative.

Noteworthy is the quite small effect of the fluorine substitution in **1b** and **1c** (30 and 80 mV, respectively) compared with dye **1a** and the larger increase (210 mV) upon substitution with four chlorine atoms (**1d**). Dye **1e** with the tetrabrominated perylene core has the highest reduction potential in this series, although bromine possesses the smallest electronegativity in this row of halogens.

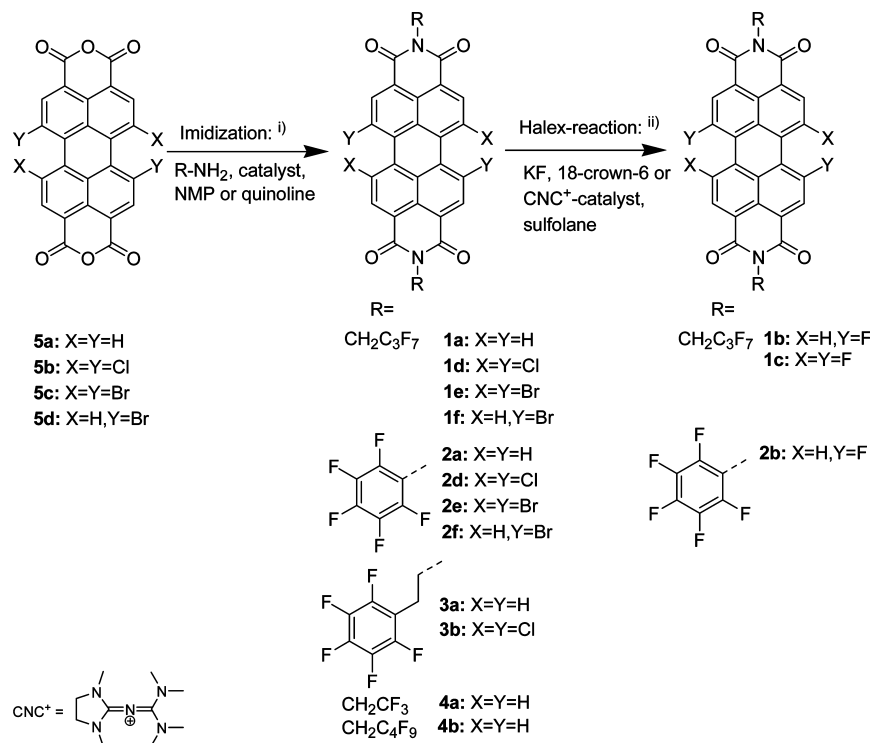
The dyes of series **2** bearing pentafluorophenyl substituents in the imide position can be reduced more easily than PBIs **1** as indicated by their first reduction potentials, ranging from -0.88 V (**2a**) to -0.64 V (**2e**). Accordingly, the perfluorinated phenyl substituents withdraw electron density from the perylene core. This effect has also been observed previously for perylene bisimide dyes with fluorine-free aromatic and aliphatic imide substituents.²⁷ The overall trend in the reduction potentials within this series is similar to that of series **1**, and the tetrabrominated PBI **2e** is the most electron-deficient dye among all PBI derivatives investigated in this work. The reduction potentials of PBIs **3a** and **3b** are in between the values for alkyl and perfluoroalkyl-methylene substituted PBIs. The redox properties of **4b** are very similar to those of **1a**.

Examination of the Packing in the Solid State. To achieve a proper understanding of the arrangement of the molecules in the solid state and its consequences for materials properties,

- (19) Oh, J. H.; Liu, S.; Bao, Z.; Schmidt, R.; Würthner, F. *Appl. Phys. Lett.* **2007**, *91*, 212107.
- (20) Könemann, M.; Osswald, P.; Schmidt, R.; Würthner, F. WO Patent 2007093643, 2007.
- (21) Katz, H. E.; Lovering, A. J.; Johnson, J.; Kloc, C.; Slegrist, T.; Li, W.; Lin, Y.-Y.; Dodabalapur, A. *Nature (London)* **2000**, *404*, 478–481.
- (22) Ling, M.-M.; Erk, P.; Gomez, M.; Könemann, M.; Locklin, J.; Bao, Z. *Adv. Mater.* **2007**, *19*, 1123–1127.
- (23) Qiu, W.; Chen, S.; Sun, X.; Liu, Y.; Zhu, D. *Org. Lett.* **2006**, *8*, 867–870.
- (24) Würthner, F.; Stepanenko, V.; Chen, Z.; Saha-Möller, C. R.; Kocher, N.; Stalke, D. *J. Org. Chem.* **2004**, *69*, 7933–7939.

- (25) (a) Pleschke, A.; Marhold, A.; Schneider, M.; Kolomeitsev, A.; Röschenthaler, G.-V. *J. Fluorine Chem.* **2004**, *125*, 1031–1038. (b) Würthner, F.; Osswald, P.; Schmidt, R.; Kaiser, T. E.; Mansikkämäki, H.; Könemann, M. *Org. Lett.* **2006**, *8*, 3765–3768.
- (26) Seguy, I.; Jolinat, P.; Destrule, P.; Mamy, R.; Allouchi, H.; Couseille, C.; Cotrait, M.; Bock, H. *ChemPhysChem* **2001**, *2*, 448–452.
- (27) Salbeck, J.; Kunkely, H.; Langhals, H.; Saalfrank, R. W.; Daub, J. *Chimia* **1989**, *43*, 6–9.

Scheme 1. Synthetic Routes of PBIs 1–4^a



^a (i) Imidization of the bisanhydrides **5a–d** with the corresponding amines to obtain PBI s **1a,d–f**, **2a,d–f**, **3a,b**, and **4a,b**. (ii) Halex reaction of PBI s **1d,f** and **2d,f** to obtain fluorinated PBI s **1b,c** and **2b**; for detailed conditions see Supporting Information.

Table 1. Half-Wave Reduction Potentials (in V versus Fc/Fc^+) of 1–4 in Dichloromethane and Calculated LUMO Energies of All Soluble Derivatives

compd	$E(\text{PBI}/\text{PBI}^-)$ (V) ^a	$E(\text{PBI}^-/\text{PBI}^{2-})$ (V) ^a	ϵ_{LUMO} (eV) ^b
1a	-0.95	-1.15	-3.85
1b	-0.92	-1.14	-3.88
1c	-0.87	-1.12	-3.93
1d	-0.74	-0.95	-4.06
1e	-0.70	-0.91	-4.10
2a	-0.88	-1.08	-3.96
2b	-0.86	-1.08	-3.94
2d	-0.69	-0.89	-4.11
2e	-0.64	-0.84	-4.16
3a	-1.01	-1.21	-3.79
3b	-0.81	-1.02	-3.99
4b	-0.96	-1.15	-3.84
1b*	-1.04	-1.25	-3.76

^a Measured in 0.1 M solution of Bu₄NPF₆ in dichloromethane, scan rate of 100 mV/s, ferrocene served as internal standard. ^b Determined according to literature methods: $\epsilon_{\text{LUMO}} = -4.8 \text{ eV} - (E(\text{PBI}/\text{PBI}^-))$.²⁶

crystallization experiments of all derivatives were carried out and five single crystals of series **1** (**a–e**) and two single crystals of series **2** (**b, d**) suitable for X-ray diffraction could be obtained after several crystallization attempts. Solvent-free single crystals of compounds **1a–c**, **2b**, and **2d** were obtained by recrystallization from benzene (or toluene) or slow diffusion of methanol into chloroform solution, respectively. Single crystals of perylene bisimide dyes **1d** and **1e** of sufficient quality were very difficult to obtain, as the pronounced twisting of the aromatic systems led to inclusion of solvent molecules. Hence, no solvent-free crystals could be obtained, and benzene molecules were embedded in both structures. The detailed crystallographic data are given in the Supporting Information.

By measuring the $\pi-\pi$ distance (d), the pitch angle (P), and roll angle (R) (Figure 1), the longitudinal (along N–N axis)

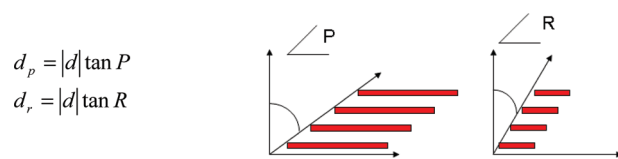


Figure 1. Definition of the pitch angle (P) and roll angle (R) according to Curtius.²⁸

and transverse (short molecular axis) shifts of the dyes **1a**, **1b**, and **1c** were calculated according to Curtius et al.²⁸

Perylene bisimide **1a** crystallizes in the triclinic space group $P\bar{1}$, and the unsubstituted molecule shows a nearly planar π -system with a torsion angle of only 1.5° in the bay position (C7–C8–C10–C11). The shortest C–C bonds (1.38 \AA) can be found in the perylene core between C2–C6 and C4–C12. The longest C–C bond within the perylene core is found, as expected,²⁹ between the two naphthalene units (C8–C10, Figure 2) and corresponds to a $C(sp^2)$ – $C(sp^2)$ single bond with a length of 1.47 \AA .

In the crystal, the molecules are arranged in a slip-stacked face-to-face arrangement with a short interplanar distance of 3.31 to 3.35 Å (Figure 2), coming close to the interplanar spacing of graphite.³⁰ Within the stack a pitch angle of 46° is found, leading to a high longitudinal shift of the molecules, $d_p = 3.46$ Å (N–N distance ≈ 11.4 Å). The roll angle is moderate ($R = 20^\circ$), corresponding to a transverse shifting of only $d_r = 1.22$ Å. Given this small roll angle, the intermolecular π – π overlap is estimated to be 50%. The closest contacts (2.46 Å)

- (28) Curtius, M. D.; Cao, J.; Kampf, J. W. *J. Am. Chem. Soc.* **2004**, *126*, 4318–4328.
 (29) Graser, F.; Hädicke, E. *Liebigs Ann. Chem.* **1980**, 1994–2011.
 (30) Forrest, S. R.; Kaplan, M. L.; Schmidt, P. H. *J. Appl. Phys.* **1984**, *55*, 1492–1507.

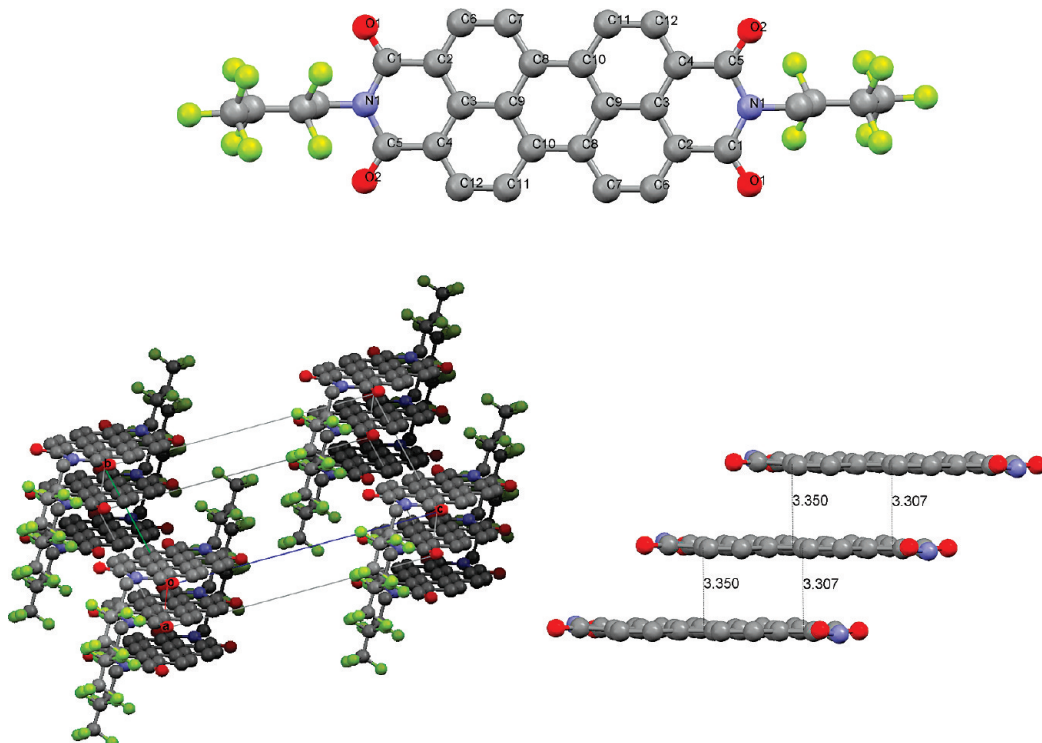


Figure 2. Single crystal structure with labels (top), packing with cell axis (left), and distances in the stacks (right, for clarity only the perylene part is shown) of **1a**.

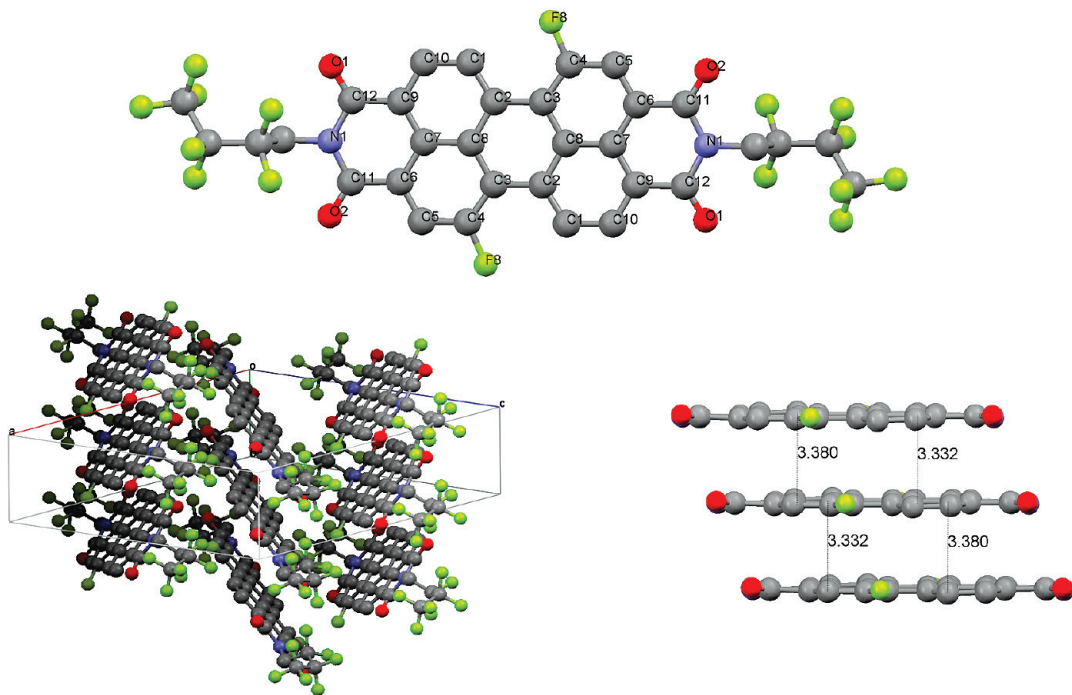


Figure 3. Single crystal structure with labels (top), packing with cell axis (left), and side view on the stacks of **1b** (right, for clarity only the perylene part is shown).

between the perylene stacks can be found among the aromatic hydrogen atoms and the oxygen atoms of the imide groups. This interaction contributes to a dense packing of the molecules within the crystal ($\rho = 1.889 \text{ g/cm}^3$).

The difluorinated PBI derivative **1b** crystallizes in the monoclinic space group $P2_1/c$. Given the small van der Waals radius of the fluorine atoms, the planarity of the molecules is not changed and the torsion angle in the bay area is only slightly

increased up to 3.0° . Nevertheless, the solid state packing changes drastically from a slipped stack to a typical “herringbone” structure with a short interplanar spacing of 3.33 \AA within each stack (Figure 3, left). According to Curtius et al.²⁸ a herringbone structure can be observed when two adjacent molecular stacks have a roll angle in the opposite direction. The pitch angle of 22° results in a longitudinal shift of about $d_p = 1.37 \text{ \AA}$, significantly smaller than that for **1a**. A

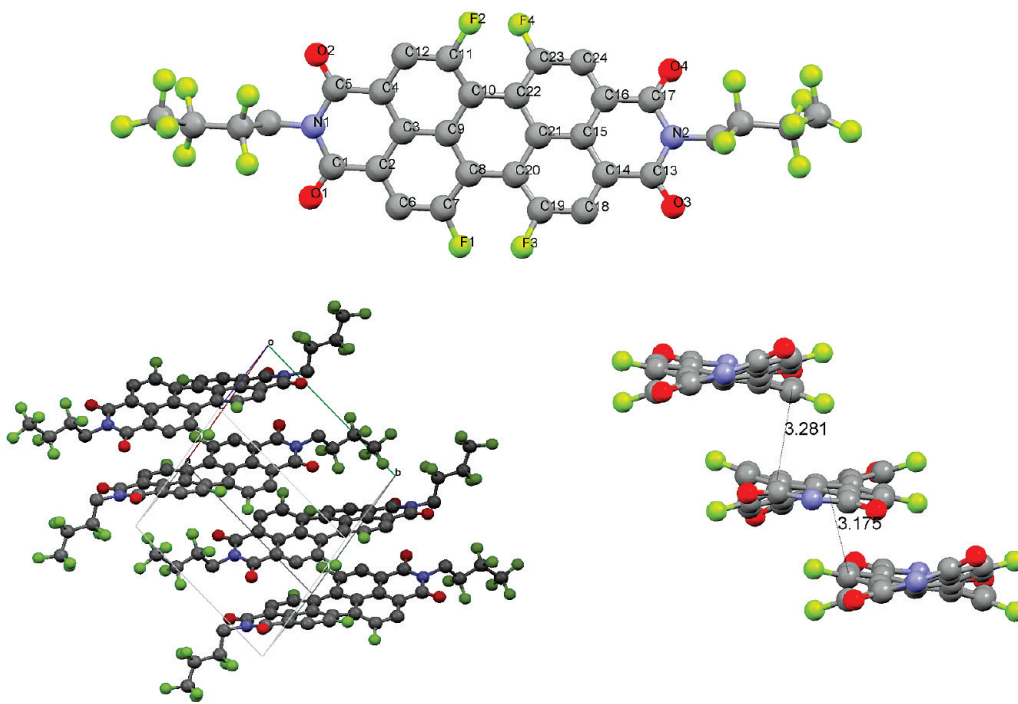


Figure 4. Single crystal structure with labels (top), packing with cell axis (left), and side view on the stacks (right, for clarity only the perylene part is shown) of **1c**.

roll angle of 48° provokes a large transverse shift of $d_r = 3.63$ Å and reduces the direct $\pi-\pi$ overlap to less than $\sim 5\%$. These observations are typical for herringbone arrangements, and the intermolecular interactions between adjacent stacks seem to outmatch interactions within the individual stacks. The closest intermolecular distances (2.49 Å) are found between a hydrogen atom in the bay position of the perylene core and a fluorine atom of the alkyl chain of a neighboring molecule.

This different arrangement might be due to a different quadrupole moment of the dyes upon attachment of two additional fluorine atoms in the bay position. Another contribution to the different packing (compared to **1a**) clearly stems from repulsion between electron-rich elements like oxygen and fluorine. Though this “herringbone” arrangement might not be ideal to achieve high electron mobilities, the calculated density of this crystal structure is the highest (1.995 g/cm³) within the series **1** and **2**.

The tetrafluorinated perylene bisimide **1c** crystallizes in the triclinic space group *P*1 with a calculated density (1.884 g/cm³) similar to that of compound **1a**. The repulsive interactions between the four fluorine atoms in the bay position distort the planar π -system which results in a twisting of the two naphthalene subunits. Due to packing effects and molecular interactions in the crystal lattice, each molecule has two different dihedral angles in the bay area, 19.8° and 25.1° , respectively. Also, two molecules with opposite chirality are observed in the crystal structure in a 1:1 ratio; i.e., a racemate is given in the solid state. These atropisomers (*M* and *P* enantiomers) are only stable in the solid state due to the low barrier of interconversion in solution.¹⁵ Although the naphthalene subunits of neighboring molecules are still orientated parallel to each other, two different minimum distances (3.18 and 3.28 Å, respectively) are observed along the stack (Figure 4, left). Such alternating packing of *M* and *P* enantiomers are typical for core-tetrasubstituted perylene

bisimide dyes.^{25,31} Obviously, dimer pair formation occurs preferentially when the crystallographic repeat distance is doubled due to the occurrence of two different enantiomers within the stacks. For this crystal structure, the two sets of pitch and roll displacement parameters can only be measured with a certain inaccuracy due to the twisting of the chromophores and their partly nonparallel arrangements. For two molecules with $d = 3.28$ Å, a pitch angle of 61° and a roll angle of 43° were found, leading to a longitudinal shift of $d_p = \sim 6.0$ Å and a transverse shift of 3.1 Å. For molecules with a closer distance ($d = 3.18$ Å) a pitch angle of -16° (angle contrariwise to the main stacking direction) and a roll angle of 49° were found, exhibiting a longitudinal shift of $d_p = \sim -0.9$ Å and a transverse shift of 3.6 Å. These very high displacement parameters lead to negligible $\pi-\pi$ contact between neighbored molecules.

Single crystals of **1d** could only be grown in aromatic solvents like benzene. This PBI derivative crystallizes in the monoclinic space group *C*2. As expected, the four large chlorine atoms in the bay position lead to high torsion angles of 34.8° and 36.4° . Surprisingly, the carbon–carbon bond length connecting the naphthalene subunits is rather small (1.43 and 1.44 Å), even shorter than that for the unsubstituted dye **1a**. In addition, the crystal structure contains dye and benzene molecules stacked along the crystallographic *b* direction (Figure S2). Embedding of the solvent molecules prohibits reasonable conclusions regarding the structure of vacuum deposited thin films of this material in OTFT devices.

Derivative **1e** crystallizes in the monoclinic space group *C*2. Just as in the case of **1d**, the crystal contains embedded benzene molecules between the perylene cores. Interestingly, the torsion angle (37.2°) increases only slightly compared to that of the tetrachlorinated compound **1d**, in agreement with computational predictions based on AM1 calculations.¹⁵ Given the similar

(31) Chen, Z.; Debije, M. G.; Debaerdemaeker, T.; Osswald, P.; Würthner, F. *ChemPhysChem* **2004**, 5, 137–140.

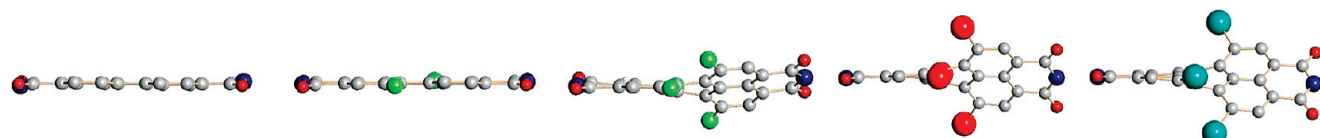


Figure 5. Side view onto the aromatic systems of **1a–e** (from left to right) showing a progressive twist of the perylene core. The angles are 1.5° for **1a**, 3.0° for **1b**, 19°/26° for **1c**, 35°/36° for **1d**, and 37° for **1e**.

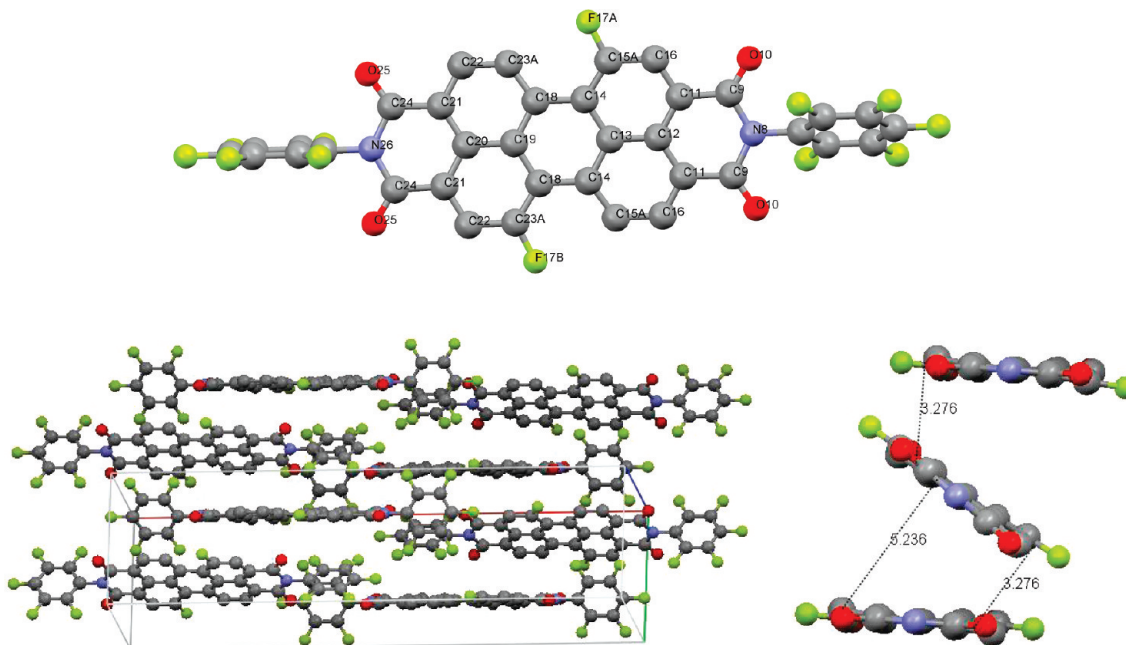


Figure 6. Single crystal structure with labels (top), “brickstone”-like packing with cell axis (left), and distances in the stacks (right) of **2b**.

torsion angle and molecular structure, the solid state structure of **1e** closely resembles that of **1d**. Overall, the measured structures agree very well with the proposed nonlinear increase of the torsion angles¹⁵ (Figure 5). Although the van der Waals radius of the bromine substituents is much larger than that of chlorine atoms, the increase of the torsion angle upon substitution by space-filling substituents indicates that the “saturation level” is already reached at the stage of chlorine.

The solid state packing of the derivatives **2b** and **2d** differs significantly from that usually observed for structurally related perylene bisimides. Derivative **2b** crystallizes in the orthorhombic space group *Pnna* and the difluorinated perylene core has a similar molecular structure to that of **1a** or **1b**. Therefore, the completely different packing of **2b** must be assigned to the effect of the perfluorinated aromatic imide substituents that are rotated out of the perylene plane.

Despite the nonplanarity of the molecules, system **2b** adopts a side shifted brickstone-like packing (Figure 6, left) which still allows for close $\pi-\pi$ contacts of less than 3.28 Å (Figure 6, right) due to an angulated arrangement of the perylene backbones. However, the $\pi-\pi$ overlap of vicinal PBI molecules is rather small, and only the bisimide groups have a significant overlap with the neighboring π -surface. The angulated arrangement of the dye molecules leads to a low density (1.821 g/cm³) of the crystal, much lower than that found for PBI derivatives **1a–e**.

The tetrachlorinated perylene bisimide **2d** crystallizes in the triclinic space group *P\bar{1}*, and the perylene core is quite similar to that for **1d** with torsion angles of 36.7° and 35.8°. As already found in other solvent-free crystal structures of tetrasubstituted

PBIs, a 1:1 composition of *M* and *P* enantiomers with different distances (3.51 and 3.37 Å, Figure S3, left) can be observed.

The combination of the highly twisted aromatic core and the bulky imide substituents (torsion angles between 62° and 70°) makes $\pi-\pi$ interactions even more difficult. Compared with **2b**, the molecules of **2d** show a larger transverse shift in the crystal structure, resulting finally in a side-shifted columnar arrangement. The nearest neighbors within one stack exhibit only a small $\pi-\pi$ overlap of ~10%; the overlap with the second vicinal PBI is even smaller. Both the formation of dimeric pairs and the small $\pi-\pi$ overlap in crystals grown from this material are expected to reduce charge carrier mobility.

OTFT Measurements. Top-contact/bottom-gate configuration OTFT devices, in which the source and drain electrodes are vacuum-deposited on top of the semiconductor film, have been prepared to investigate the electrical performance of the synthesized PBI molecules (Figure 7a). OTFT devices were prepared on a SiO₂ (300 nm thickness, capacitance $C_i = 10$ nFcm⁻²) dielectric with the underlying n-doped silicon as the gate electrode. The SiO₂ surface was treated with *n*-octadecyl triethoxysilane [C₁₈H₃₇Si(OC₂H₅)₃; OTS] in vapor phase (herein, this surface treatment will be denoted as OTS-V), as described previously (the experimental details are given in the Supporting Information).²² The PBI semiconductors were vacuum-deposited to form thin films (45 nm thickness). Subsequently, gold was deposited on top of the semiconductor film through a shadow mask to form source and drain electrodes (the typical channel length was 50 μ m, and the width/length ratio was ~20).

In OTFT operation, a bias voltage applied to the gate electrode modulates the accumulation of charges in the semiconductor

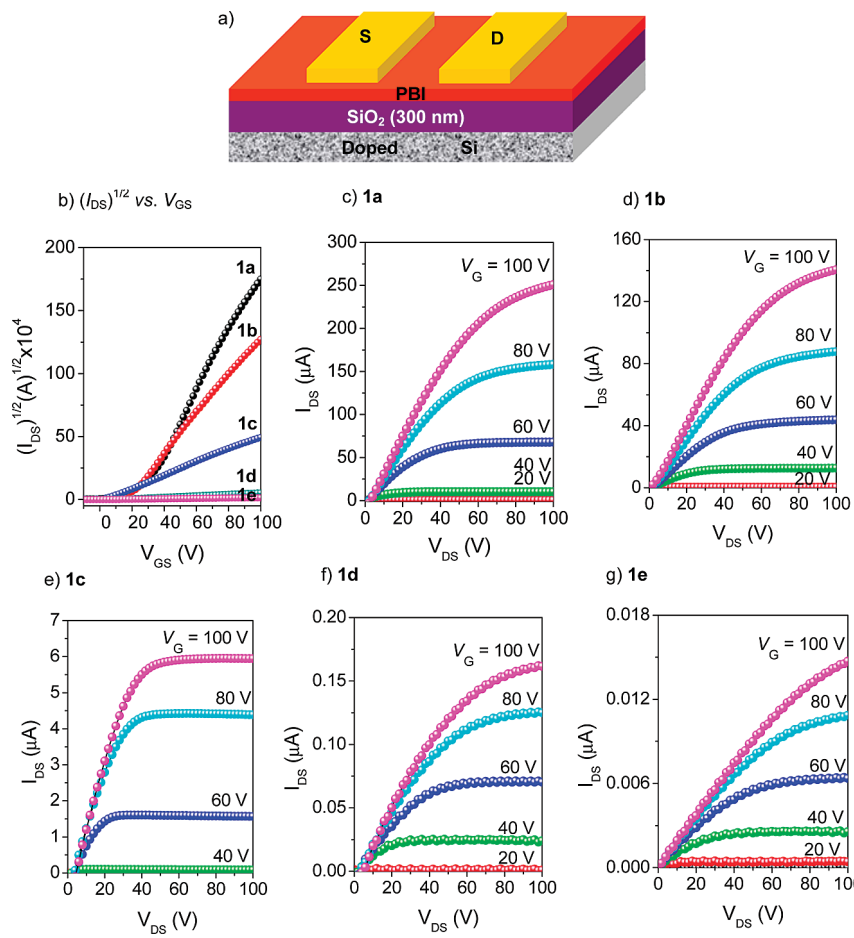


Figure 7. OTFT device structure and representative OTFT I – V characteristics of series **1** compounds. (a) Top-contact/bottom-gate OTFT device structure, (b) comparison of the plots of $(I_{DS})^{1/2}$ vs V_{GS} for the OTS-V treated OTFT devices of series **1** compounds, and representative output characteristics of (c) **1a**, (d) **1b**, (e) **1c**, (f) **1d**, and (g) **1e**.

layer near the interface with the dielectric. In a typical n-channel operation mode, a positive gate voltage bias induces the accumulation of electron carriers and, hence, current flows in the channel between source and drain electrodes. The TFT performance parameters, such as charge carrier mobility (μ), on-to-off current ratio (I_{on}/I_{off}), and threshold voltage (V_t), were extracted from the drain–source current (I_{DS}) vs gate–source voltage (V_{GS}) characteristics under the assumptions of conventional transistor equations.³² The mobilities were determined in the saturation regime from the slope of plots of $(I_{DS})^{1/2}$ versus V_{GS} . TFT characteristics were measured in a nitrogen-filled glovebox (oxygen level <1 ppm) as well as under ambient environment (the relative humidity ~50%) at ~1 h after exposing the TFT devices to air. Figure 7b exhibits the plots of $(I_{DS})^{1/2}$ versus V_{GS} for the OTS-V treated OTFT devices based on compounds **1a**–**e**. The output characteristics showing I_{DS} vs drain–source voltage (V_{DS}) for different gate biases measured under nitrogen atmosphere reveal that each compound possesses well-defined linear and saturation regimes (Figure 7c–g). The transfer characteristics of series **1** compounds are shown in Figure S4.

Table 2 summarizes the OTFT performance data of the devices prepared on the OTS-V treated SiO_2/Si substrates. The substrate temperature (T_D) was chosen as 125 °C, since this temperature falls within the purview of the optimized substrate

temperature for the PBI derivatives.¹⁹ (For details, refer to the discussion on the influence of substrate temperature.)

The highest mobility among the PBI compounds was observed for compound **1a**, which showed a charge carrier mobility as high as $0.72 \text{ cm}^2 \text{ V}^{-1} \text{ s}^{-1}$. As discussed earlier, the single crystal of **1a** has a slip-stacked face-to-face molecular packing with close contacts of 3.31 Å between the PBI π -planes. This close distance of undistorted PBI cores allows a very dense and parallel arrangement of the molecules, leading to high charge carrier mobility. As the substitution grade of core halogenation in series **1** compounds increases, the field-effect mobility decreases. The compound **1b** (pure 1,7 regioisomer) containing two fluorine atoms in the bay region embraces a herringbone structure and exhibits about half of the mobility of core-unsubstituted **1a**. It is worth noting that OTFT devices prepared from 1,7- and 1,6-regioisomeric mixture (about 9:1) of **1b** exhibited equally good performance as in the case of the pure 1,7 isomer. The torsion angle of the PBI π -conjugated core in compound **1b** is still small (3.0°), whereas that in compound **1a** is only 1.5°, resulting in a virtually planar π -system desirable for efficient charge carrier transport. On the other hand, for compound **1c**, the repulsive interactions between the four fluorine atoms in the bay position severely distort the π -system leading to stacks composed of alternating atropisomers (*M* and *P* enantiomers). As a result of the less dense and less regular packing, the field-effect mobility of compound **1c** is 1 order of magnitude smaller than that for **1b**. This trend clearly reveals

(32) Sze, S. M. *Semiconductor Devices*; John Wiley & Sons: New York, 1985; p 523.

Table 2. OTFT Performance Data^a for the PBI-Based Devices Prepared on the SiO₂ Wafers with Vapor Phase Treated OTS (OTS-V) Layer at the Substrate Temperature of 125 °C

compd	N ₂ atmosphere			air			
	μ (cm ² V ⁻¹ s ⁻¹)	I_{on}/I_{off}	V _t (V)	μ (cm ² V ⁻¹ s ⁻¹)	I_{on}/I_{off}	V _t (V)	$\Delta\mu$ (%) ^b
1a	0.67 ± 0.05 (0.72) ^c	10 ⁵	14–29	0.51 ± 0.05 (0.56)	10 ⁶	28–43	23.9
1b	0.35 ± 0.01 (0.36)	10 ⁷	10–24	0.33 ± 0.02 (0.35)	10 ⁶	16–34	5.7
1c	0.030 ± 0.002 (0.032)	10 ⁵	1–18	0.029 ± 0.002 (0.031)	10 ⁶	5–37	3.3
1d	(4.6 ± 0.4) × 10 ⁻⁴ (5.0 × 10 ⁻⁴)	10 ³	5–17	(3.9 ± 0.3) × 10 ⁻⁴ (4.2 × 10 ⁻⁴)	10 ³	7–24	15.2
1e	(2.5 ± 0.4) × 10 ⁻⁵ (2.9 × 10 ⁻⁵)	10 ³	2–20	(2.2 ± 0.5) × 10 ⁻⁵ (2.7 × 10 ⁻⁵)	10 ³	5–22	12.0
2b	0.029 ± 0.014 (0.041)	10 ⁵	2–8	0.021 ± 0.007 (0.028)	10 ⁶	12–26	27.6
2d	0.025 ± 0.012 (0.037)	10 ⁶	9–15	0.020 ± 0.006 (0.026)	10 ⁶	17–35	20.0
3a	0.31 ± 0.02 (0.33)	10 ⁶	5–14	0.29 ± 0.02 (0.31)	10 ⁷	7–19	6.5
3b	(2.0 ± 0.3) × 10 ⁻⁵ (2.2 × 10 ⁻⁵)	10 ³	7–10	(6.1 ± 0.5) × 10 ⁻⁶ (2.2 × 10 ⁻⁵)	10 ⁴	26–35	69.5
4a	0.029 ± 0.002 (0.031)	10 ⁶	9–15	0.010 ± 0.006 (0.016)	10 ⁵	12–24	65.5
4b	0.081 ± 0.006 (0.087)	10 ⁶	19–29	0.065 ± 0.006 (0.071)	10 ⁶	24–39	19.8
1b*	0.09 ± 0.02 (0.11)	10 ⁶	20–29	not stable in air			

^a The mobilities were determined in the saturation regime from the slope of plots of (I_{DS})^{1/2} vs V_{GS} . The I – V measurements in N₂ atmosphere were carried out inside a glovebox filled with nitrogen (oxygen level <1 ppm), whereas the measurements in air were performed under ambient laboratory conditions (the relative humidity ~50%) ~1 h after exposing the devices to air. ^b Percentage drop of the average mobility after taking devices out of the glovebox to air. ^c The mobility in the parentheses represents the maximum recorded mobility.

that the core substitution can drastically change the crystal packing motif and, hence, the corresponding charge transport. As the data in Table 2 reveal, however, the smallest drop of the average mobility was observed upon exposure to air for compound **1c** with additional fluorine substituents at the core.

Compounds **1d** and **1e** bearing more bulky chlorine and bromine atoms at the PBI core exhibited much less field-effect mobilities compared to fluorine-substituted derivative **1c**. This is presumably due to the significantly increased torsion angles and the reduced intermolecular π – π interactions that hinder efficient charge transport. In addition, the brominated PBI **1e** may not be stable during the vacuum deposition due to decomposition at elevated temperature. We note that another tetrachloroperylene bisimide derivative showed higher charge carrier mobility (up to 0.11 cm² V⁻¹ s⁻¹),²² indicating that the charge transport is highly sensitive toward molecular packing features. Likewise, for the tetrachloro PBI backbone, the replacement of perfluorinated alkyl side chains by perfluorinated aromatic groups in the imide position improves the charge carrier mobility by ~2 orders of magnitude (see the performances of compounds **1d** and **2d** in Table 2). It is remarkable that OTFT devices based on **2d** exhibit high field-effect mobility despite the highly twisted aromatic core and the bulky imide substituents (Figure S3). The perfluorinated aromatic imide substituents may provide an additional charge transport path for the tetrachloro-substituted PBIs. In addition, the vacuum-deposited thin films most likely adopt a packing motif different from the solvent-embedded single crystals. On the other hand, for the core-undistorted compounds containing two fluorine atoms at the PBI core (**1b** and **2b**), the additional substitution of perfluorinated aromatic groups in the imide position did not improve the field-effect mobility.

Compound **3a**, which possesses an alkyl spacer between perfluorinated phenyl and imide nitrogen, showed a field-effect mobility as high as 0.33 cm² V⁻¹ s⁻¹. Considering the TFT performance of **2a** (0.06 cm² V⁻¹ s⁻¹),¹³ the two bridging ethyl spacers in the planar core compounds give reasonably good hope of improving the intermolecular π – π interactions, presumably by endowing the perfluorinated aromatic groups with flexibility to enable enhanced π -orbital overlap. However, these spacers in the twisted core system were not helpful in enhancing the

mobility of core-twisted PBI compounds (see performances of **2d** and **3b**). Extension or reduction of the fluorocarbon unit in the perfluoroalkyl side chains deteriorated the mobility of core-undistorted PBIs as revealed by the OTFT performances of **1a** and **4a,b**. As the chain length of the perfluorinated alkyl substituents is reduced, the air stability decreases drastically (see the percentage drops of the average mobility of **1a** and **4a**). This might be explained with the kinetic barrier mechanism^{1a,b,12–14,19} for the air stability of n-channel OTFT devices. The relatively smaller segregated fluoro domains in compound **4a** might be insufficient for providing an efficient barrier against the diffusion of oxygen and moisture into the active channel area. OTFT devices of compound **1b*** are not stable in air, probably due to their relatively high LUMO level and absence of segregated fluoro domains.

Effect of SiO₂ Surface Treatment on OTFT Performance. Typically, the OTS-V treated substrates provided 1 to 3 orders of magnitude higher mobilities compared to the bare SiO₂/Si substrates. This is primarily attributed to the reduced charge trapping at the dielectric/semiconductor interface of OTS-V treated substrates.^{9b,19,22} AFM analysis reveals that the grains on OTS-V treated substrates are much larger and have well-defined thin film morphology, compared to those on bare substrates, which is consistent with higher mobility in the OTS-V treated substrates (Figure S5). Charge transport takes place predominantly in the first few monolayers of an organic semiconductor near the semiconductor/dielectric interface in an OTFT device.³³ It has been reported that the phase state³⁴ and the density³⁵ of the modification layer of the dielectric surface play an important role in controlling the growth and crystallinity of pentacene thin films. To investigate the effect of phase and density of OTS layer on the OTFT performance of the PBI

(33) (a) Dodabalapur, A.; Torsi, L.; Katz, H. E. *Science* **1995**, 268, 270–271. (b) Dinelli, F.; Murgia, M.; Levy, P.; Cavallini, M.; Biscarini, F.; Leeuw, D. M. D. *Phys. Rev. Lett.* **2004**, 92, 116802. (c) Ruiz, R.; Papadimitratos, A.; Mayer, A. C.; Malliaras, G. G. *Adv. Mater.* **2005**, 17, 1795–1798.

(34) Lee, H. S.; Kim, D. H.; Cho, J. H.; Hwang, M.; Jang, Y.; Cho, K. *J. Am. Chem. Soc.* **2008**, 130, 10556.

(35) Virkar, A.; Mannsfeld, S.; Oh, J. H.; Toney, M. F.; Tan, Y. H.; Liu, G.-Y.; Scott, J. C.; Miller, R.; Bao, Z. *Adv. Funct. Mater.* **2009**, in press.

Table 3. OTFT Performance Data for the PBI-Based Devices Prepared on the SiO₂ Wafers with Solution Phase Treated, Highly Ordered OTS (OTS-S) Layer^a

compd	N ₂ atmosphere			air			
	μ (cm ² V ⁻¹ s ⁻¹)	$I_{\text{off}}/I_{\text{eff}}$	V_t (V)	μ (cm ² V ⁻¹ s ⁻¹)	$I_{\text{off}}/I_{\text{eff}}$	V_t (V)	$\Delta\mu$ (%) ^b
1a	1.42 ± 0.03 (1.44) ^c	10 ⁶	39–47	1.18 ± 0.05 (1.24)	10 ⁶	47–57	16.9
1b	0.64 ± 0.02 (0.66)	10 ⁶	9–15	0.58 ± 0.03 (0.61)	10 ⁶	11–29	9.4
1c	0.054 ± 0.004 (0.058)	10 ⁶	1–16	0.052 ± 0.004 (0.056)	10 ⁶	4–22	3.7
1d	(3.5 ± 0.7) × 10 ⁻⁵ (4.2 × 10 ⁻⁵)	10 ³	8–17	(2.5 ± 0.8) × 10 ⁻⁵ (3.3 × 10 ⁻⁵)	10 ³	14–25	28.6
1e	(4.1 ± 1.2) × 10 ⁻⁵ (5.3 × 10 ⁻⁵)	10 ³	6–15	(3.1 ± 0.8) × 10 ⁻⁵ (3.9 × 10 ⁻⁵)	10 ³	11–23	24.4
2b	0.76 ± 0.06 (0.85)	10 ⁷	8–14	0.45 ± 0.06 (0.51)	10 ⁷	17–41	40.8
2d	0.28 ± 0.07 (0.38)	10 ⁷	19–23	0.21 ± 0.06 (0.27)	10 ⁷	17–33	25.0
3a	0.59 ± 0.03 (0.62)	10 ⁶	21–29	0.33 ± 0.04 (0.37)	10 ⁷	28–39	44.1
4a	0.044 ± 0.005 (0.049)	10 ⁶	9–18	0.020 ± 0.003 (0.023)	10 ⁷	18–28	54.5
4b	0.10 ± 0.01 (0.11)	10 ⁶	20–34	0.083 ± 0.009 (0.092)	10 ⁶	25–37	17.0
1b*	0.53 ± 0.14 (0.74)	10 ⁷	19–28	(4.6 ± 3.5) × 10 ⁻² (7.7 × 10 ⁻²)	10 ⁵	45–59	91.3

^a The substrate temperature was 125 °C, with the exception of **1d** where T_D was 90 °C (no film was deposited from **1d** at 125 °C due to desorption). The I-V measurements and the data analysis were performed under the same conditions as for Table 2. The highly ordered OTS was treated in solution phase (for experimental details, see Supporting Information). ^b Percentage drop of the average mobility after taking devices out of the glovebox to air.

^c The maximum mobility is denoted in the parentheses. **3b** did not show any field effect on OTS-S substrate.

derivatives, we also modified the surface of the bare SiO₂ dielectric with highly ordered OTS in solution phase³⁵ (OTS-S; the experimental procedures are described in Supporting Information, and a comparison of the properties of OTS-V and OTS-S layers is given in Table S3).

The OTFT performance data of the PBI-based devices prepared on OTS-S substrates are collected in Table 3. The OTFT devices prepared on OTS-S substrates at a T_D of 125 °C showed higher field-effect mobility compared to those on OTS-V substrates, with the exception of **1d** and **3b**. No film of **1d** was obtained on the OTS-S substrate due to desorption at a T_D of 125 °C, and the performance of **1d** lists the OTFT data at a T_D of 90 °C. PBI **3b** did not show any field effect on the OTS-S substrate at a T_D of 125 °C. The field-effect mobility of compound **1a** is as high as 1.44 cm² V⁻¹ s⁻¹ on the OTS-S substrate. Such significant improvement (a factor of ∼2) was also observed for **1b** and **3a**, both of them exhibiting field-effect mobilities >0.5 cm² V⁻¹ s⁻¹. Compound **2b** showed the largest improvement on the OTS-S substrate (0.76 cm² V⁻¹ s⁻¹; 26 times larger) compared to those prepared on the OTS-V substrate. AFM analysis of **2b** thin films prepared with a nominal thickness of 3 nm reveals that there are huge differences in the thin film growth mode on different surfaces (Figure 8). On the highly ordered OTS-S substrate, a larger coverage of the first layer is observed, which results in a more smooth thin film. On the other hand, lower nucleation density and a more extended 3D growth are observed on the OTS-V substrate that leads to a rough thick film, which tends to have poor connections between grains. On the bare SiO₂ surface even more pronounced 3D growth is formed, resulting in a very rough thick film.

The observed OTFT mobilities correlate well with the film morphology.³⁶ Thus, for the more rough 3D film on the bare substrates, a very low field-effect mobility of 1.1×10^{-6} cm² V⁻¹ s⁻¹ was observed for **2b**, while the field-effect mobilities of the OTFTs prepared on OTS-S were improved by ∼700 000 times, compared with the mobilities of those prepared on bare substrates. Our results demonstrate that the nucleation and growth of PBI semiconductor thin films are highly sensitive to the nature of the dielectric surface and a highly ordered and

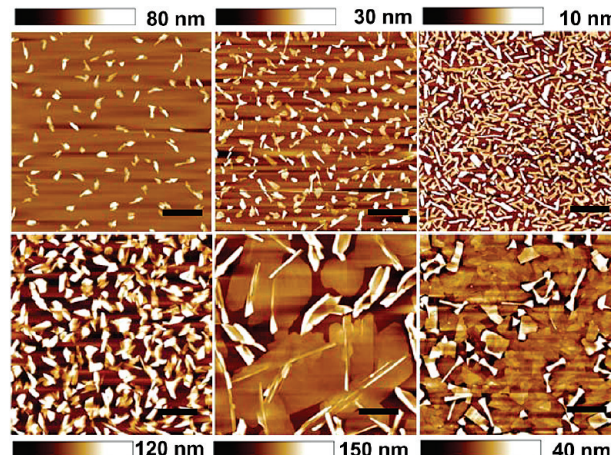


Figure 8. AFM topography images of compound **2b** thin films on different surfaces: bare (left), OTS-V (middle), OTS-S (right) SiO₂/Si substrates with a nominal thickness of 3 nm (top) and 45 nm (bottom), respectively. The scale bar displays 2 μm. The thin films were deposited under identical conditions as used in TFT fabrication (0.3 Å/s at 125 °C).

dense OTS surface modification layer facilitates 2D semiconductor film growth, leading to enhanced charge carrier mobility.

Influence of the Substrate Temperature on OTFT Performance

In general, the substrate temperature (T_D) used for deposition of organic semiconductor thin films plays an important role in the OTFT performance by influencing the nucleation and growth of the organic semiconductor molecules.^{8b,13,14,19} To explore the optimal T_D , thin films of compound **1a** were fabricated at different substrate temperatures. Figure 9 shows the effect of T_D on the grain size and the OTFT performance. The grain size was estimated by averaging the length of the long axis from ∼20 grains. As the T_D increased from 25 to 140 °C, the average grain size in the thin film increased from 160 nm to more than 2 μm. The field-effect mobility was also enhanced with increasing T_D . However, an optimized T_D value is given for the maximum mobility. Under our experimental conditions, the maximum mobility of compound **1a** was observed at 125 °C. As the T_D increased further, the mobility began to decrease. At a T_D of 150 °C, only a few devices showed an FET behavior with a maximum mobility of 0.13 cm² V⁻¹ s⁻¹ and many other devices did not exhibit any transistor behavior. AFM analysis

(36) Verlaak, S.; Steudel, S.; Heremans, P.; Janssen, D.; Deleuze, M. S. *Phy. Rev. B* **2003**, 68, 195409.

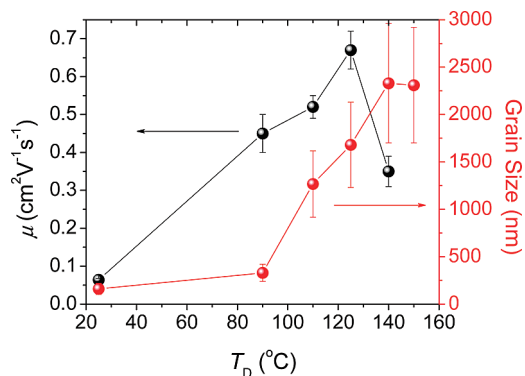


Figure 9. Effect of substrate temperature (T_D) on the grain size and the OTFT performance of **1a** thin films. The grain size as estimated by measuring the average length of long axis of ~ 20 grains.

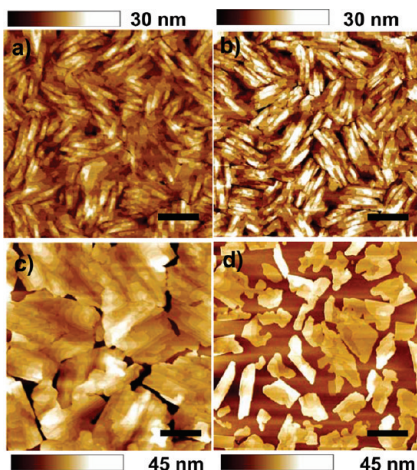


Figure 10. AFM images of 45 nm thickness thin film of compound **1a** prepared at a different substrate temperature: (a) 110, (b) 125, (c) 140, (d) 150 °C. The scale bar represents 2 μm .

on the thin films prepared at the transition temperatures revealed that the gaps between the grains increased significantly and the crack formation was severe at a substrate temperature over 125 °C (Figure 10). The significant crack formation at a T_D of 150 °C is presumably due to the high tension exerted on the organic thin film upon cooling from such an elevated temperature, which originates from the large difference in the thermal expansion coefficient between the SiO_2 substrate and the organic semiconductor thin film.^{8b}

Most of the remaining PBI compounds, except **1d** and **2a**, showed their maximum mobility at a T_D of 125 °C. As described previously, no film was deposited from compound **1d** on OTS-S at 125 °C due to the surface dewetting. Chen et al. reported that the best OTFT performance of compound **2a** on the OTS-V substrate was obtained at a relatively low substrate temperature of 75 °C, while most of the other PBI derivatives exhibited their best performance at ~ 125 °C.¹³

Air Stability of the PBI OTFT Devices. Compared to positive charge (hole) carriers, the negative charge (electron) carriers in organic semiconductors are more easily trapped at interfaces such as the semiconductor/gate dielectric interface or at grain boundaries within the semiconductor. These traps are known to be generated by ambient oxidants such as oxygen, water, or ozone.^{9,10,14} Therefore, a large number of n-channel organic semiconductors hereby only work in vacuum or under an inert atmosphere.

In general, two main factors are important for air stability of n-channel OTFT devices: (i) redox potential to prevent ambient oxidation^{9,11,12b,37} and (ii) dense solid state packing to create kinetic barriers to slow down the diffusion of ambient oxidants into the active channel area.^{1a,b,14,19,38} Jones et al. reported that resistance to charge carrier trapping under ambient conditions for *N*-(*n*-octyl)arylene bisimide films occurs at a molecular reduction potential more positive than ~ -0.1 V versus SCE (LUMO ~ -4.3 eV).^{9a} They estimated that the overpotential for the reaction of PBI n-type charge carriers with ambient oxygen in arylene imide films is ~ 0.6 V, implying that air-stable OTFT devices are in principle achievable with properly designed arylene cores having appropriate electron-withdrawing substituents. Rylene dyes containing perfluorinated substituents in the imide position showed remarkable air stability for n-channel OTFT operation, although the fluorinated side chains do not significantly alter the LUMO energy levels ($\Delta E \leq 0.15$ eV). Katz et al. suggested that the larger van der Waals radius of a fluorine atom relative to a hydrogen atom leads to a decrease of available space between the *N,N'*-chains from approximately 4 to 2 Å, thus kinetically hindering O_2 intrusion.^{12a}

More recently, Weitz et al. reported that these conventional interpretations are not sufficient to explain the air stability of their PBI films. They found that the rate of mobility degradation in air was independent of the degree of molecular order in core-cyanated PBI films.¹⁰ They have proposed that a mechanism which is neither related to the redox potential nor to the kinetic barrier is responsible for the air stability.

Although they have come up with new insights into the air stability of n-channel OTFT devices, they used core-cyanated PBI molecules with relatively low LUMO levels that fall under the empirical reduction potential windows required for air stability.³⁷ In addition, since there is a possibility that a zigzag brick-type packing of the PBI molecules with their long axis arrangement parallel to the surface may also provide a kinetic barrier to the oxidants, it is still not clear whether the same degradation rate is completely independent of the LUMO levels and the kinetic barrier. On the other hand, it is also uncertain, to what extent the empirical chemical reduction potential window for air stability can be generalized to interpret the air stability of various types of n-channel organic semiconductors, since the reduction potentials for thin films are different from those measured in solution.

Considering the background on the air stability of n-channel organic semiconductors, we have tested the air stability of PBI OTFT devices. Figure 11 depicts the percentage drop of the average mobility after exposing the devices on OTS-V and OTS-S substrates to air (relative humidity $\sim 50\%$) for 1 h as a function of the LUMO level of PBI compounds. For high performance PBI compounds (**1a–c**) with $\text{CH}_2\text{C}_3\text{F}_7$ side chains, the mobility drop reduces with increasing core fluorination, presumably due to the lowering of LUMO and the enhanced electron affinity. However, tetrachloro functionalization at the PBI core was not helpful in reducing the mobility drop, despite the effective lowering of LUMO levels as can be seen for the pairs **1a**, **1d** and **3a**, **3b**. The significantly twisted backbones of these tetrachloro-functionalized PBIs may lead to less dense packing and facile intrusion of ambient oxidants by the structural imperfection, which is also consistent with the significantly reduced charge carrier mobilities for these tetrachloro PBI compounds. The air stability of these PBI OTFTs seems to be governed by complex interplays between the LUMO level (electron affinity) and solid state packing.

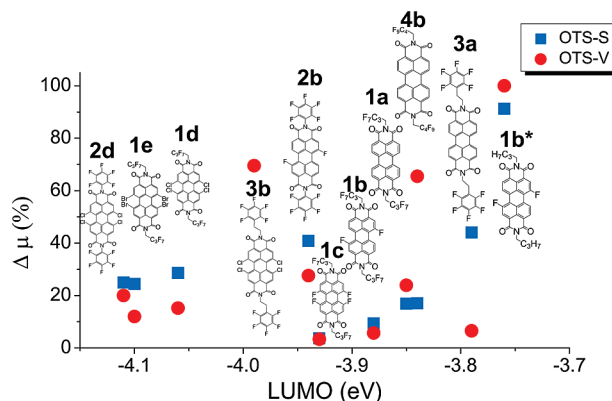


Figure 11. Percentage drop of average mobility ($\Delta\mu$) after exposing the PBI OTFT devices to air (relative humidity $\sim 50\%$) for 1 h as a function of the LUMO level of PBI molecules. Blue squares and red circles represent OTS-S and OTS-V devices, respectively.

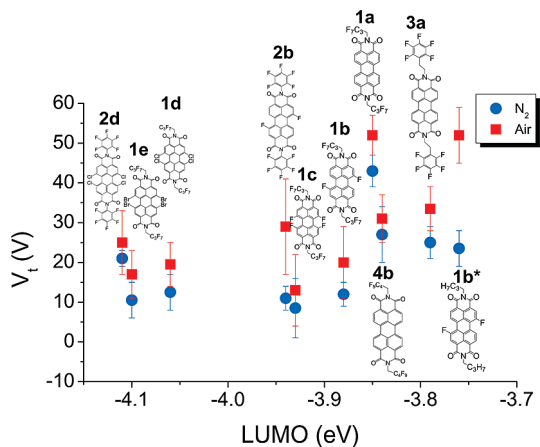


Figure 12. V_t values of OTFT devices prepared on OTS-S substrates as a function of LUMO level of the PBI compounds after exposing the devices to air (relative humidity $\sim 50\%$) for 1 h. Blue circles and red squares represent the V_t values in nitrogen and air, respectively.

The performance of the OTFT device based on **1b*** without fluorinated side chains rapidly degrades in air. Judging from the empirical reduction potential window for air stability,^{14,37} the LUMO levels of **1a** and **1b*** are quite high, corresponding to the onset region of air stability. However, they displayed very different air stabilities. In addition, **1b*** OTFT devices on OTS-V and bare SiO₂/Si substrates did not work at all in air, whereas those on the OTS-S substrate have at least functioned, although the degradation (91.3%) of the TFT performance was fairly large. Our observations clearly demonstrate that the fluorinated side chains in the imide position play an important role in air stability, and the difference in molecular packing and the film growth mode can affect the degradation rate of n-channel OTFTs.

Figure 12 shows the V_t shift of OTFT devices prepared on OTS-S substrates as a function of the LUMO level of the PBI molecule after exposing the devices to air for 1 h. For all of the OTFT devices, the V_t increased in air as a result of ambient traps.^{8b,9,19} Most of the PBI OTFT devices exhibited a V_t shift of less than +10 V in air, while **1b*** OTFT device showed a V_t shift of $\sim +30$ V. The degree of V_t shift corresponds well with the percentage drop of mobility.

The long-term air stability was monitored by measuring the TFT performance as a function of time for the higher mobility compounds **1a**, **1b** and **2b**, **2d** (Figure 13 and Figure S6). The

field-effect mobility of the OTFT device prepared from compound **1a** decreased from 0.63 to 0.48 cm² V⁻¹ s⁻¹ immediately after taking the device out of a nitrogen-containing glovebox, but no further decrease was observed for ~ 2 months. An OTFT device prepared from **1b** showed excellent air stability without any decrease in performance within 15 days. These results indicate that the trap sites are saturated right after exposing the devices to air through the structural defects such as grain boundaries and gaps. Further degradation is significantly delayed owing to the fluorinated side chains which can prevent the intrusion of ambient oxidants physically and/or electrostatically. On the other hand, the increased electron affinity of the PBI π -conjugated core achieved by core fluorination appears to endow more resistance to the ambient oxidation in the initial stage. The OTFT devices based on **2b** and **2d** also showed long-term air-stable n-channel operations (Figure S6). For **1a** and **2b**, the I_{on}/I_{off} of the OTFT devices in air improved compared with those under inert atmosphere because the off-current decreased by an order of magnitude in air. This presumably originates from the oxidation of unintentionally doped PBI radical anions in air.¹⁹ These PBI OTFTs exhibited very high on-to-off current ratios (typically 10^7 to 10^8) in air, which is 2 to 3 orders of magnitude higher than those usually reported for PBI derivatives. The excellent on-to-off current modulation combined with high mobility makes this class of semiconductors very promising for a wide range of practical applications.

GIXD Measurements of Thin Films. To directly correlate molecular structure and packing with charge transport properties, it is crucial to obtain the detailed structure of the organic semiconductor in the thin film form. GIXD measurements have been carried out to investigate the molecular packing of the vacuum-deposited PBI thin films. GIXD utilizes small incident angles for the incoming X-ray beam, and thus diffraction can be made surface sensitive and thin film unit cell structures can be defined.^{39,40}

Out-of-plane d -spacings provide information on the molecular orientations relative to the substrate surface. For most small molecule organic semiconductors, the optimal orientation for efficient charge transport between source and drain electrodes is considered to be the perpendicular arrangement of the π -conjugated cores relative to the dielectric surface.^{9,41} Out-of-plane d -spacings and the tilting angles relative to the surface plane normal, estimated from the PM3 geometry-optimized molecular lengths, are listed in Table 4. The GIXD data indicate that highly ordered/layered microstructures are formed for all the PBI thin films investigated here.

We analyzed the lattice parameters in the vacuum-deposited thin films for the high-performance PBI compounds including **1a–c** and **1b*** (see Figure S7 for their GIXD patterns). The GIXD patterns of **1a,b** and **1b*** showed well-defined, high intensity diffraction patterns. PBI **1c** showed more complicated diffraction patterns, presumably related to the alternating distances along the stacking direction due to the presence of

- (37) Wang, Z.; Kim, C.; Facchetti, A.; Marks, T. J. *J. Am. Chem. Soc.* **2007**, *129*, 13362–13363.
- (38) Katz, H. E.; Johnson, J.; Lovinger, A. J.; Li, W. J. *J. Am. Chem. Soc.* **2000**, *122*, 7787–7792.
- (39) Yuan, Q.; Mannsfeld, S. C. B.; Tang, M. L.; Toney, M. F.; Lüning, J.; Bao, Z. *J. Am. Chem. Soc.* **2008**, *130*, 3502–3508.
- (40) Krauss, T. N.; Barrena, E.; Zhang, X. N.; de Oteyza, D. G.; Major, J.; Dehm, V.; Würthner, F.; Cavalcanti, L. P.; Dosch, H. *Langmuir* **2008**, *24*, 12742–12744.
- (41) (a) Horowitz, G. *J. Mater. Res.* **2004**, *19*, 1946–1962. (b) Sun, Y.; Liu, Y.; Zhu, D. *J. Mater. Chem.* **2005**, *15*, 53–65.

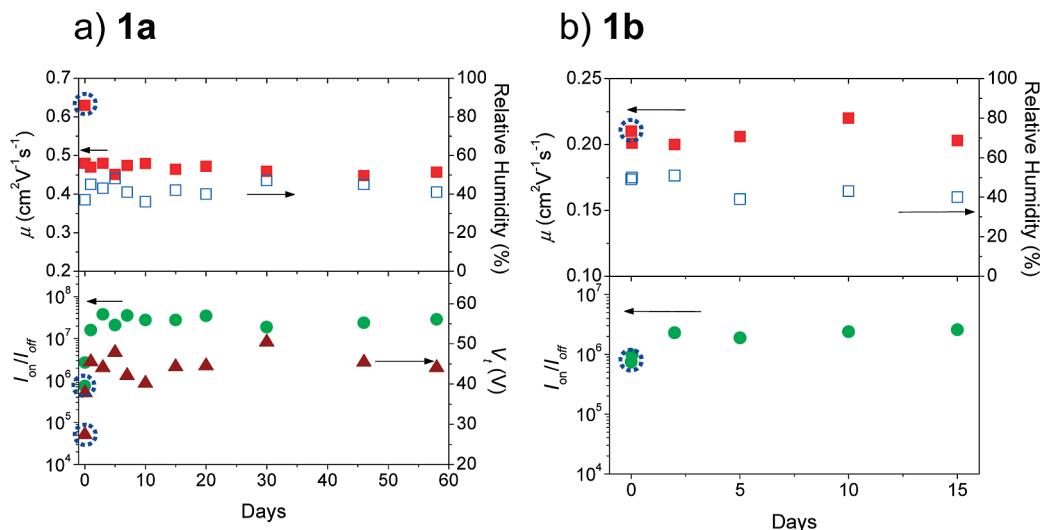


Figure 13. Air-stability measurements of PBI OTFT devices based on (a) compound **1a** (OTS-V), (b) **1b** (OTS-V). Top: μ (red solid squares) and relative humidity (blue open squares). Note that the mobilities of **1b** are slightly lower than those given in Table 2, because the devices for these air-stability measurements were constructed with as-prepared **1b** without further purification by sublimation. Bottom: I_{on}/I_{off} (green solid circles) and V_t (brown solid triangles). The dotted blue circle values at initial time correspond to the electrical performance in a nitrogen-filled glovebox. The V_t of **1b** OTFT was not recorded.

Table 4. Out-of-Plane d -Spacing Values Obtained from GIXD Measurements of the PBI Thin Films Prepared on OTS-S Treated SiO_2/Si Substrates at $T_D = 125^\circ\text{C}$ and the Estimated Tilt Angle of the Semiconductor Molecule Relative to the Substrate Plane Normal

compd	d -spacing (Å)	calculated molecular length (Å)	tilt angle (deg) ^a
1a	16.56	21.78	49
1b	14.45	22.86	39
1c	14.98	22.88	41
1e	16.99	22.68	49
2b	14.59	22.40	41
2d	12.20	22.31	33
3a	16.35	27.52	36
4a	12.96	18.70	44
4b	21.85	25.59	59
1b*	14.79	23.08	40

^a The tilting angle was estimated by using the geometry-optimized, calculated molecular lengths obtained from MM2 energy minimization and PM3 geometry optimization.

Table 5. Experimental Lattice Parameters Obtained from the GIXD Measurements of the PBI Thin Films Prepared on the OTS-S Treated SiO_2/Si Substrates at a T_D of 125°C

compd	a (Å)	b (Å)	c (Å)	α (deg)	β (deg)	γ (deg)
1a	5.10	8.81	16.77	96.70	85.21	81.61
1b	12.39	7.25	14.47	90	90	90
1c	9.66	11.35	14.99	92.43	91.68	73.95
1b*	4.88	18.24	15.04	98.68	83.59	97.13

two atropisomers (*M* and *P* enantiomers) in the single crystal form. Table 5 lists the lattice parameters of the PBI thin films. Whereas **1a**, **1c**, and **1b*** thin films have triclinic space groups, **1b** thin films possess an orthorhombic space group in which three unequal axes are formed at right angles. For **1a** and **1c** the unit cells are similar to those found in the single crystal (Table S1), while the cell parameters of **1b** thin films are quite different from the single crystal, where a monoclinic space group prevails.

It was difficult to obtain the detailed information about exact cell parameters for compounds **1e** and **2b** due to the lack of strong out-of-plane diffraction. For **2d** and **3a**, each of the two

molecules may contain a mixture of two phases. Compound **4a** appears to adopt two different types of orientations (edge-on and flat-on) on the surface, judging from two sets of out-of-plane d -spacings. In general, for vacuum-deposited thin films, the phases are much more complicated than single crystals, which are typically perfect and single-phased, and embrace well-defined three-dimensional crystal orientations. In thin films, however, the crystal growth is not perfect and the long-range crystal ordering is inferior.

Conclusions

In this paper we reported on a series of hitherto mostly unknown perylene bisimide (PBI) based organic semiconductors and their performance in OTFT devices on SiO_2 gate dielectrics treated with different densities of OTS layers (OTS-V and OTS-S). For several PBIs with a flat aromatic core owing to the presence of only up to two fluorine substituents at the PBI bay positions, we could obtain high-performance n-channel transistors with field effect mobilities between 0.5 and $1.44 \text{ cm}^2 \text{ V}^{-1} \text{ s}^{-1}$ and on-to-off current ratios $> 10^6$. In contrast, PBIs with a distorted aromatic core evoked by four halogen substituents (fluorine, chlorine, or bromine) at the PBI bay positions showed in general lower charge carrier mobilities and on-to-off current ratios. This inferior behavior is attributed to packing constraints arising from the distorted core that encumber the formation of extended highly crystalline grains. Accordingly, single crystals grown from solutions of these compounds typically include cocrystallized solvent molecules, while for the flat PBIs dense and solvent-free crystals were obtained that exhibit π -stacks with short interplanar distances ($\sim 3.3 \text{ \AA}$ for **1a** and **1b**). The variation of the imide substituents in the parent PBI compound (bearing no halogen substituents at the PBI core) with different perfluorinated residues afforded several derivatives with excellent electron carrier mobility and on-to-off current ratios even in air that distinguish these materials from those without fluorinated side chains (e.g., **1b***). The easy synthetic availability of these organic semiconductors from the industrial pigment perylene tetracarboxylic acid dianhydride (PTCDA) should be very beneficial for their applications as electron-transporting semi-

conductors in a wide range of organic electronic devices, including photovoltaic cells, light-emitting diodes, and OTFTs.

Acknowledgment. F.W. gratefully acknowledges financial support from BASF SE and the DFG. Z.B. acknowledges financial support from BASF SE and the Sloan Research Fellowship. J.H.O. acknowledges partial financial support from the Korea Research Foundation Grant (MOEHRD KRF-2006-352-D00066).

Supporting Information Available: General experimental information, synthetic details, and compound characterization by ^1H NMR, MS, UV-vis absorption and fluorescence

spectroscopy, and cyclic voltammetry for all PBIs. Tables with crystallographic data for **1a–e**, **2b**, and **2d**, details on the SiO_2 substrate treatment with OTS and seven additional figures (cyclic voltammograms, crystal structures, OTFT transfer characteristics, AFM topography and GIXD patterns of thin films, time-dependent OTFT air stability measurements). This material is available free of charge via Internet at <http://pubs.acs.org>.

JA901077A